Indian Journal of Engineering & Materials Sciences
Vol. 27, April 2020, pp. 221-233

Mechanical properties and kinetics of boride layers on AISI D2 steel produced by plasma paste boriding

Mourad Keddam[a*], Natalia Makuch[b], Michal Kulka[b] & Andrzej Miklaszewski[b]

[a] Laboratory of Materials Technology, Faculty of Mechanical Engineering and Process Engineering, USTHB, B.P. No. 32, 16111 El-Alia, Bab-Ezzouar, Algiers, Algeria

[b]Poznan University of Technology, Institute of Materials Science and Engineering, Pl. M Sklodowskiej-Curie 5, 60-965 Poznan, Poland

Received: 05 March 2018; Accepted: 11 March 2020

In the present study, the AISI D2 steel has been treated by the plasma paste boriding process using a gas mixture of 70% H_2-30% Ar with 70% of borax and 30% SiC. The boriding treatment has been carried out at 700, 750 and 800 °C for an exposure time of 3 to 7 h. The plasma paste borided samples have been investigated by various techniques such as scanning electron microscopy, optical microscopy, XRD analysis, micro-hardness Vickers and the rockwell-C adhesion tests. The fracture toughness has also been measured on the plasma paste borided samples under different values of indentation load. From a kinetic point of view, the boride layers have obeyed the parabolic growth law. The value of boron activation energy for AISI D2 steel has been estimated as 130 kJ mol^{-1} using our experimental results. In addition, this obtained activation energy has been compared to the literature data.

Keywords: Plasma paste boriding, Kinetics, Borides, Activation energy, Adhesion test, Fracture toughness

1 Introduction

The boronizing treatment is a thermochemical surface hardening extensively employed in many industries[1]. It is a surface treatment process that enriches the surface of a workpiece by boron atoms in the temperature range 800-1050°C for a treatment time between 0.5 and 10 h. The resulting metallic borides offer high surface hardness and wear resistance as well as corrosion resistance. The boriding process can be carried out in gaseous[2], liquid[3], solid[4] and plasma media[5].

The laser boriding and laser alloying with boron can be also used as an alternative to modify the surface properties of steels. In this regard, Gopalakrishan *et al.*[6] have applied the laser – heat treatment to modify the microstructure of borided C15 steel. Kulka *et al.*[7,8] have used the laser alloying with boron to produce the boride layers on 41Cr4 and austenitic 316 L steels.

The plasma boriding possesses an outstanding advantage when compared to the traditional boriding methods. However, the use of gases such as B_2H_6 and BCl_3 *are not environment-friendly because of their toxicity*[9].

As an alternative to this boriding process, the plasma paste boriding (PPB)[10-12] was recently used to avoid the handling of poisonous gases such as B_2H_6 and BCl_3. In this process, the inert gases such as argon and hydrogen, which are harmless to the environment, can be safety employed. During the PPB process, a high energy of plasma was generated to provide lower boriding temperatures in comparison with traditional boriding processes (solid and liquid). Consequently, the distortion of treated workpieces can be reduced.

The objective of the present study was to analyze the plasma paste boriding (PPB) kinetics of AISI D2 steel in the temperature range 700-800 °C. The obained boride layers were experimentally characterized by different techniques. The Rockwell-C adhesion test was then employed to qualitatively evaluate the adhesion quality of the boride layer formed at 800 °C during 7 h on the AISI D2 steel's substrate. Furthermore, the fracture toughness was measured on the sample borided at 800 °C during 7 h under different values of indentation load. On the basis of our kinetics data, the value of boron activation energy for AISI D2 steel was estimated and a comparison was made by using the data available in the literature.

*Corresponding author (E-mail: keddam@yahoo.fr)

2 Experimental Procedure

2.1 The material and plasma paste boriding process

The AISI D2 steel was employed as a substrate for the plasma paste boriding process. Its nominal chemical composition was the following: 1.40–1.60%C, 0.30–0.60%Si, 0.30–0.60% Mn, 11.00–13.00%Cr, 0.70–1.20%Mo, 0.80–1.10%V, 0.030%P and 0.030%S and Fe balance. Cylindrical specimens with 20 mm in diameter and 5 mm in height were used. Before the plasma paste boriding, a metallographic preparation of samples was done and the samples were ultrasonically cleaned in an alcohol solution. Then, they were coated with a paste consisting of a mixture of 70% borax and 30% SiC. The boriding treatment was realized in a DC plasma system at the three temperatures 700,750 and 800 °C for 3, 5 and 7 h in a gas mixture of 70% H_2-30%Ar with a mixture of 70% borax and 30% SiC. After completing this treatment, the samples were left to cool in the chamber by using Argon gas.

During the plasma paste boriding, some chemical reactions yielding the formation of boride layers at the surface of steels are possible[13]. Under the glow discharge conditions, the borax as a source of boron reacted with the active hydrogen (H+) according to the following chemical reaction:

$$Na_2B_4O_7 + 12H+ \rightarrow Na_2O + 6H_2O + 4B \quad \text{... (1)}$$

Simultaneously, the boron hydride was formed following the chemical reaction:

$$xB + yH^+ + ye^- \rightarrow B_xH_y \quad \text{... (2)}$$

The atomic boron element was released from the paste by thermal decomposition of the produced boron hydride:

$$B_xH_y \rightarrow xB + 0.5yH_2 \quad \text{... (3)}$$

The active atomic boron reacted with iron atoms from the material surface to produce two kind of iron borides (Fe_2B and FeB). The possible chemical reactions involved are the following :

$$B^+ + 2Fe \rightarrow Fe_2B \quad \text{... (4)}$$

and

$$B^+ + Fe \rightarrow FeB \quad \text{... (5)}$$

2.2 Experimental techniques

Directly after plasma-paste boriding, the specimens were cleaned with ethanol. Then, the X-ray diffraction examination was carried out on the surface of specimen in order to identify the phases present in the boride layer. The PANalytical EMPYREAN instrument with Cu-K_α radiation at λ=1.5406Å was used for this study. The diffraction angles were taken in the range of 20° to 90°. For microstructure observation, the metallographic preparation, included following operations: cutting out across the boride layer, grinding by using emery, polishing with the application of alumina suspension, and etching, was necessary. The polished and etched cross-sections of the boride layers were examined by scanning electron microscope and an optical microscope (OM).

The etching of boronized samples was carried out with a chemical solution composed of 20 ml glycerine, 10 ml HNO_3 and 30 ml HCl for SEM observations and Nital solution for OM examinations.

Fifty measurements were performed on different locations of cross-sections of boronized layers in order to get the mean values of thicknesses. The microhardness measurements were performed in the cross-section of specimen from the boride layer to AISI D2 steel substrate using the Vickers microhardness test machine ZWICK 3212 B. The indentation load of 10 gf (0.0981 N) and a dwell time of 15 s were used during the measurements.

The method of microindentation with the use of a Vickers pyramidal diamond indenter was applied in this study in order to determine the fracture toughness of plasma-paste borided AISI D2 steel.

The schematic top view of indentation mark with cracks generated from the corners of the indentation mark was presented in Fig. 1. The following parameters were measured during fracture toughness test: half diagonal of the indentation *a*, crack length from the indentation center to the end of the crack *c*,

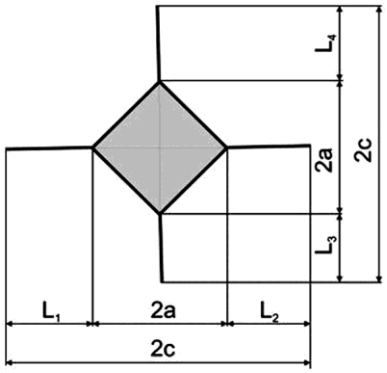

Fig. 1 — The schematic views of the obtained indentation mark with visible cracks; 2c – the total crack length, 2a – the diagonal of the indentation mark, L_1, L_2, L_3, L_4 – cracks' lengths.

crack length from the indentation corner to the end of the crack L_1, L_2, L_3, L_4. The fracture toughness of plasma-paste borided layer was calculated based on the measurements of K_C factor (in MPa·m$^{1/2}$)[14] according to Eq. (6):

$$K_C = A\frac{P}{c^{1.5}} \quad \ldots (6)$$

with

$$A = 0.028(\frac{E}{H})^{0.5}$$

P represents the load of indentation (N), c the crack length taken from the indentation center to the end of the crack (m), A the residual indentation coefficient, E *the* Young's moduli (MPa) and H *the* hardness value (MPa). In this study, Vickers microindentation fracture toughness tests were performed by means of a ZWICK 3212 B microhardness tester. Due to the low thickness of the produced plasma-paste borided layer, the measurements were carried out at the top surface of the sample. The indentation load varied from 1.96 to 9.81 N. For the calculations of K_C, the Young's moduli of FeB phase were taken, because this phase was produced near the top surface of the sample. Based on earlier paper [15], the average value of Young's moduli for FeB phase was equal to 308.86 GPa. Five measurements were taken for each indentation load. After the Vickers indentation tests, the crack lengths and the diagonals of indentation marks were measured using an optical microscope.

The cohesion of plasma-paste borided layer was measured by the Rockwell C adhesion test according to the VDI 3198 norm[16].

In this study, the Rockwell C- type diamond cone indenter was employed under a load of 150 kgf (1471 N). A schematic representation of the principle of this procedure was illustrated in Fig. 2.

During the measurements, the Rockwell-C indenter under a high load penetrated into the surface of boronized layer, causing a massive plastic deformation to the substrate and leading to the fracture of the boronized layer. After cohesion test, the indentation craters with the failure marks were examined by means of an optical microscope. The damage of the borided layer was analyzed by means of the quality maps of adhesion strength HF1–HF6 presented in VDI 3198 norm. The adhesion strength was classified on the basis of cracking level and delamination around indent. The standard HF1–HF4 corresponded to sufficient adhesion, while HF5 and HF6 were characterized by an insufficient adhesion.

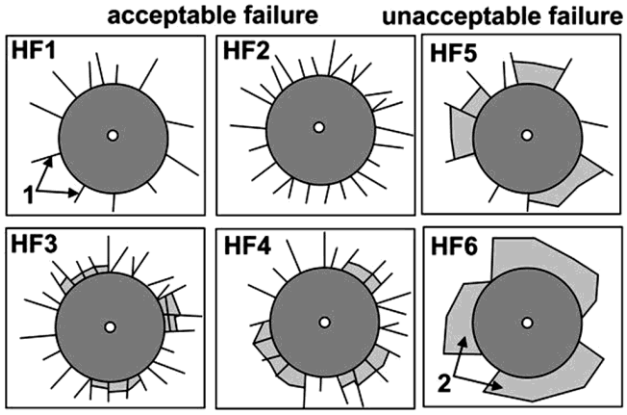

Fig. 2 — Classification map of the acceptable and unacceptable failures based on typical indentation results, according to VDI3198 standard; 1 – radial cracks, 2 – delamination.

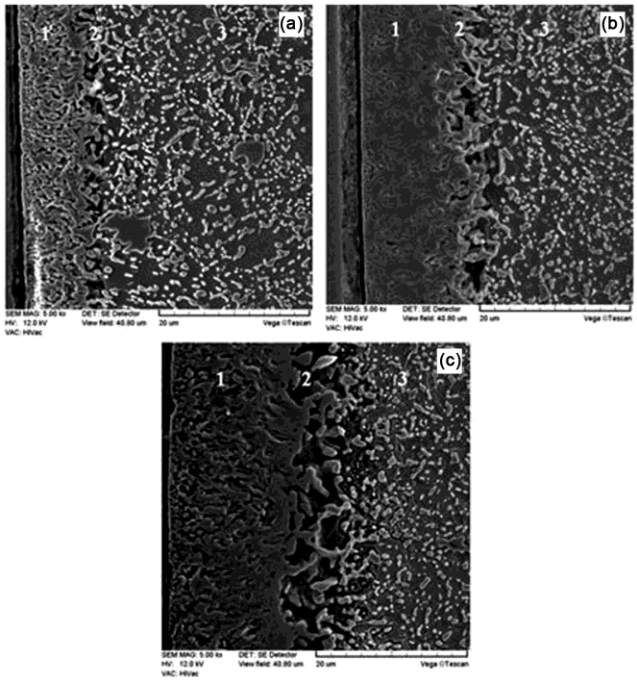

Fig. 3 — SEM micrographs of the cross-sections of boride layers formed on the AISI D2 steel for 7 h of treatment at increasing temperatures (a) 700 °C , (b) 750 °C and (c) 800°C 1 – Boride layer , 2 – Transition zone, 3 – Matrix.

3 Experimental Results and Discussion

3.1 SEM observations of boride layers

Figure 3 shows the SEM micrographs of the cross-sections of borided samples of AISI D2 steel at 700, 750 °C and 800 °C for an exposure time of 7 h. The formed boronized layers look as continuous and dense. A flat interface was observed at the (boride layer/transition zone) interface because of effect of alloying elements. In fact, the presence of alloying elements in AISI D2 steel reduced the active boron

flux in the diffusion zone. For 7 h of treatment, the boride layer thickness increased with increasing temperature. The thickness of boronized layer attained a value of 20.5 μm for the thermochemical treatment carried out at 800°C for an exposure time of 7 h whereas the boride layer was only 7.9 μm thick after the process at 700 °C for 7 h.

3.2 XRD analysis

The X-ray diffraction patterns of the plasma-paste borided AISI D2 steel confirmed the existence of two kinds of iron borides (FeB, Fe_2B) and chromium boride CrB. The XRD spectrum originated from the top-surface of boronized sample was shown in Fig. 4.

It is seen that many diffracting peaks were ascribed to FeB phase since it was a dominant phase. Moreover, the strongest reflections in XRD patterns also derived from Fe_2B phase. The nominal content of chromium in AISI D2 steel ranged from 11.00 to 13 wt %. Therefore, as a result of plasma-paste boriding, the chromium boride CrB was formed. It is known that the both borides (FeB and CrB) crystallize in the orthorhombic structure and have a tendency to give rise to a composite or mixed boride phase. Therefore, often it not easy to perform the adequate phase analysis[17]. In this study, two peaks could be also identified as both FeB and CrB phases. The analysis of literature data indicated, that in case of some boriding methods other phases could appeared.

For example, boriding in B_4C powder[18] resulted in the formation of MoB, V_2B, Mo_2B_4 phases. However, diffraction peaks corresponding to these phases were characterized by low intensity in comparison with iron borides. It was found that chromium and vanadium tend to dissolve in the boride layer, whereas molybdenum displays a much lower tendency to dissolve in the boride layer[18].

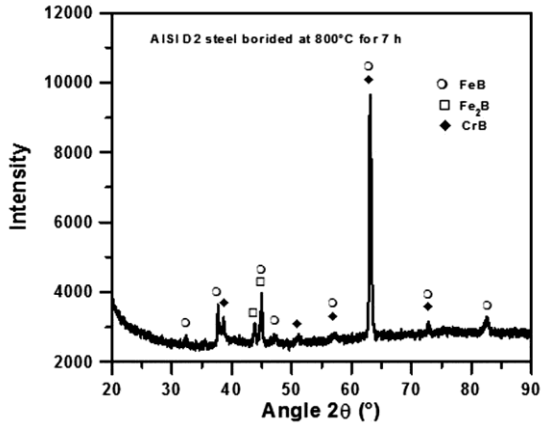

Fig. 4 — X-ray diffraction pattern of the plasma-paste borided AISI D2 steel at 800 °C for 7 h.

3.3 OM observation of boride layers

The OM microstructure of cross-sections of plasma-paste borided sample (at 800 °C for 7 h), and etched by 2% Nital solution, was shown in Fig. 5. The microstructure of produced layer revealed strong zonation. First, near the top surface the FeB zone (1) was formed. This zone was characterized by high average thickness of 13.32 μm. However, some authors[17] indicated that the first zone included also chromium boride CrB. The second zone (2), containing the Fe_2B phase, appeared below the first one. The average depth of this zone was equal to 7.17 μm. At the boundary between borided layer and substrate material, the transition zone (3) was clearly visible in Fig. 5. Probably, in this zone the carbon atoms accumulated. This situation could be caused by two phenomena. First, during the boriding process the carbon was pushed towards the substrate matrix. Second, carbon was characterized by insolubility in the boride phases. The transition zone reached over an average thickness of 10.8 μm. Below the transition zone, the AISI D2 steel's substrate (4) was visible. The chemical composition of AISI D2 steel strongly influenced the morphology of boride layer. The presence of a high Cr content in AISI D2 steel diminished the diffusion rate of boron atoms into the workpiece by forming a smooth layer. In reference to the research papers[19-21], when the chromium concentration in steel increased, the formed boronized layers were thinner with a flat interface between the boronized layer and the substrate. It was difficult to compare the thickness of the plasma-paste borided AISI D2 steel to the literature data due to the differences in the boriding methods as well as in the process parameters used during the boriding

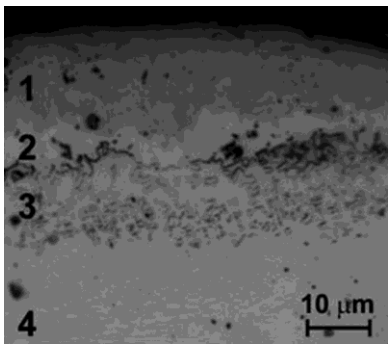

Fig. 5 — OM microstructure of the plasma-paste borided AISI D2 steel at 800 °C for 7 h; 1 – FeB zone, 2 – Fe_2B zone; 3 – transition zone, 4 – substrate.

treatment. However, based on literature data[17,18,22,23], it could be concluded that plasma-paste boriding at 800°C for 7 h resulted in the formation of a very thick FeB zone. The amount of FeB zone in total layer thickness was about 65 %. This value is higher in comparison with e.g. powder-pack boriding method[18,24] in which the percentage of FeB phase in total thickness was less than 50 %. Based on the literature results displayed in Table 1, the thickness of boride layers produced on AISI D2 tool steel strongly depended on the method of boriding and parameters of process. It could be found that salt bath boriding (in molten mixture consisted of borax, boric acid and ferro-silicon)[23] and electrochemical boriding (in molten borax with current density of 200 mA cm^{-2})[17] were the appropriate methods which gave rise to thick layers. Especially, the use of electrochemical boriding

Table 1 — The comparison of thickness, phase composition, hardness and fracture toughness of borided layers produced using different boriding methods.

Ref.	Method of boriding	T (°C)	Time (h)	Thickness (μm)	Phase composition	Hardness	K_c ($MPa \cdot m^{1/2}$)
18	Powder-pack boriding (B_4C powder)	950	3	Total: 24	-	FeB: 24 GPa Fe_2B: 20.5 GPa	FeB: 2.33 Fe_2B: 2.76
			5	FeB: 21 Total: 40	-	FeB: 22.8 GPa Fe_2B: 21.5 GPa	FeB: 2.82 Fe_2B: 3.09
			7	-	-	FeB: 22 GPa Fe_2B: 21 GPa	FeB: 1.60 Fe_2B: 2.01
		1000	3	-	-	-	FeB: 1.48 Fe_2B: 4.56
			5	FeB: 26 Total: 61	-	-	FeB: 1.57 Fe_2B: 2.72
			7	-	FeB, Fe_2B, CrB, Cr_2B, MoB, V_2B, Mo_2B_4	-	FeB: 1.50 Fe_2B: 2.93
		1050	3	-	-	-	FeB: 1.72 Fe_2B: 3.47
			5	FeB: 28 Total: 63	-	-	FeB: 3.04 Fe_2B: 3.80
			7	Total: 106	-	-	FeB: 2.76 Fe_2B: -
22	Powder-pack boriding (Ekabor 2 powder)	900	2	Total: 13	-	1801±20 $HV_{0.05}$	-
			4	Total: 29	FeB, Fe_2B, CrB		
			6	Total: 35	-		
		950	2	Total: 31	-	1916±55 $HV_{0.05}$	-
			4	Total: 44	FeB, Fe_2B, CrB		
			6	Total: 67	-		
23	Salt bath boriding (borax, boric acid, ferro-silicon)	850	2	Total: 20	FeB, Fe_2B, CrB, Cr_2B	1500-2140 $HV_{0.05}$	-
			4	Total: 24			
			6	Total: 28			
			8	Total: 40			
		900	2	Total: 50			
			4	Total: 57			
			6	Total: 68			
			8	Total: 80			
		950	2	Total: 88			
			4	Total: 123			
			6	Total: 155			
			8	Total: 170			
		1000	4	Total: 120	FeB, Fe_2B, CrB, Fe_3B, Cr_2B_3	1616 $HV_{0.05}$	-

(*Contd*.)

Table 1 — The comparison of thickness, phase composition, hardness and fracture toughness of borided layers produced using different boriding methods. (*Contd*.)

Ref.	Method of boriding	T (°C)	Time (h)	Thickness (μm)	Phase composition	Hardness	K_c ($MPa \cdot m^{1/2}$)
17	Electrochemical boriding (molten borax with current density of 200 mA cm^{-2})	950	0.25	FeB+CrB: 13.5 Total: 5.56	FeB, Fe_2B, CrB	1714±200 $HV_{0.05}$	-
			0.5	FeB+CrB: 20 Total: 32.93			
			0.75	FeB+CrB: 22 Total: 39.96			
			1	FeB+CrB: 42 Total: 60.35			
This work	Plasma-paste boriding (70%Borax+ 30%SiC)	800	7	FeB: 12.08 Total: 17.91	FeB, Fe_2B, CrB	FeB: 1652-2131 $HV_{0.01}$ Fe_2B: 1355-1604 $HV_{0.01}$	0.504-5.706 (depending on indentation load)

method led to the formation of a relatively thick boride layers (25.56 μm) in a very short process duration (only 15 min)[17]. The use of conventional powder agents [18,22] required increased temperature (up to 1050°C) and longer time duration (up to 7 h). Despite this, the obtained total layer thickness was even two times lower when compared with liquid boriding methods[17,23]. The presence of chromium borides is characteristic for the layers produced on AISI D2 steel, which was compiled in Table 1. Independent on boriding technique, the chromium boride CrB occurred in the microstructure of boride layers. However, some authors[18,22] reported that increase in the boriding temperature was the reason for the formation of other types of borides for example Cr_2B, MoB, V_2B, Mo_2B_4, Fe_3B, Cr_2B_3.

3.4 Microhardness profile

Microhardness measurements were carried out versus the distance from the surface, across the FeB, Fe_2B and transition zones towards to the substrate on the plasma paste borided sample at 800°C for 7 h. The low thickness of borided layer and high brittleness of iron borides were the reason for applying of a low indentation load (10 gf) during hardness measurements. The OM microstructure and micro-hardness profile of plasma-paste borided AISI D2 steel was presented in Fig. 6. As it was expected, the maximum microhardness in the range 1652-2131 $HV_{0.01}$ was obtained for FeB zone (1). Whereas, Fe_2B phase (2) was characterized by lower hardness (1355-1604$HV_{0.01}$). Below the compact iron borides' zone in transition zone (3) microhardness considerably decreased (489-367 $HV_{0.01}$). Simultaneously, the lowest hardness (316-321 $HV_{0.01}$) was characteristic for substrate material (4). The obtained results were comparable with the hardness of borided layers produced with the use of other acceptable methods of boriding summarized in Table 1.

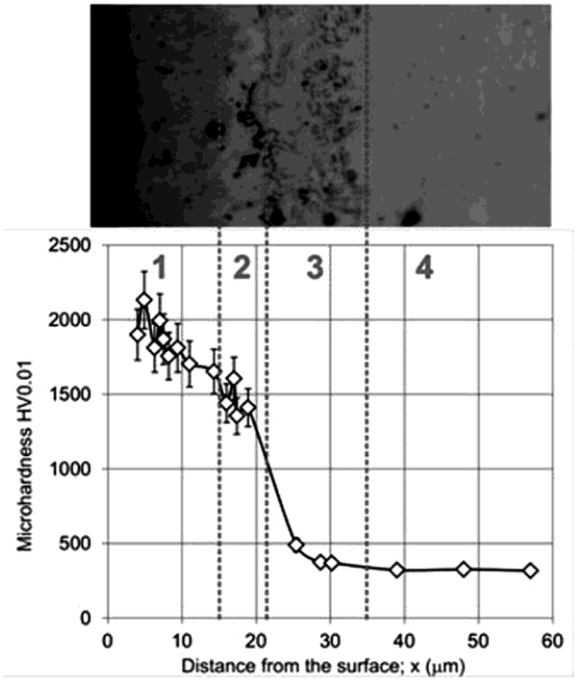

Fig. 6 — OM microstructure and microhardness profile of the plasma-paste borided AISI D2 steel; 1 – FeB zone, 2 – Fe_2B zone; 3 – transition zone, 4 – substrate.

It was clearly visible from Table 1 that the method and parameters used for boriding of AISI D2 tool steel strongly influenced on the phase composition and on measured hardness in boride layer. Near the

top-surface, the presence of FeB and CrB phases yielded the highest hardness. Simultaneously, in the second zone (Fe_2B phase) the lower hardness was measured.

3.5 Fracture toughness

In this study, the radial-median cracks were generated by Vickers indentation to estimate the fracture toughness. These cracks were detected in FeB phase. The radial-median cracking mode was characterized by the proportionality of the c value to $P^{2/3}$ value. It was confirmed by the preliminary study in which the measurements of c value were performed at various loads. The measurements of fracture toughness were carried out at the top-surface of the plasma-paste borided AISI D2 steel (at 800°C for 7 h). The following values of indentation load were applied: 1.962 N, 2.943 N, 3.924 N, 4.905 N, 6.867 N and 9.810 N. After producing of indentation marks, the lengths of cracks (L_1, L_2, L_3, L_4) and the diagonals of the indentation mark ($2a$) were measured by using an optical microscope. Based on obtained values, the hardness HV and fracture toughness K_c were calculated. The results were respectively presented in Tables 2, 3, 4 and 5, for the corresponding values of indentation load: 1.962 N, 3.924 N, 4.905 N and 9.810 N. In case of applied low indentation load (1.962 N), the cracks generated from the corners of indentation marks were characterized by high length up to 65.6 μm when compared to the diagonals length of indentation marks (Fig. 7). The average fracture toughness was equal to 2.278 MPa·$m^{1/2}$.

The increase in indentation load caused diminishing of fracture toughness for average value of 1.789 MPa·$m^{1/2}$ for indentation load of 3.924 N, respectively. In this case, the cracks' lengths were significantly lower (Fig. 8) in comparison to those generated for applied load of 1.962 N (see Fig. 7).

The interesting situation was the unexpected increase in fracture toughness for indentation marks produced by using of an indentation load above 4.905 N. However, it should be noticed that the measurements were carried out on the top-surface of specimen,

Table 2 — Results of measurements (Vickers hardness, L_1, L_2, L_3, L_4 - cracks' lengths, crack lengths from the center of the indentation to the end of the crack C, fracture toughness K_c and penetration depth h) for the indentations obtained with use of load of 1.962 N.

Indentation	HV	Cracks' lengths		C (μm)	K_c (MPa·$m^{1/2}$)	h (μm)
		L_1(μm)	L_2(μm)			
		L_3 (μm)	L_4 (μm)			
1	2411	21.6	56.8	45.6	0.64463	2.51
		12.0	0	10.8	5.70605	
2	2128	24.8	44.8	41.6	0.78753	2.67
		0	49.6	56.0	0.50423	
3	2491	16.0	65.6	46.6	0.61392	2.47
		4.8	7.2	12.4	4.47261	
4	2263	11.2	30.4	27.2	1.44441	2.59
		9.6	4.8	13.6	4.08541	
5	2128	9.6	0	16.4	3.18157	2.67
		16.8	25.6	27.6	1.45728	

Table 3 — Results of measurements (Vickers hardness, L_1, L_2, L_3, L_4 - cracks' lengths, crack lengths from the center of the indentation to the end of the crack C, fracture toughness K_c and penetration depth h) for the indentations obtained with use of load of 3.924 N.

Indentation	HV	Cracks' lengths		C (μm)	K_c (MPa·$m^{1/2}$)	h (μm)
		L_1(μm)	L_2(μm)			
		L_3 (μm)	L_4 (μm)			
1	2288	0	0	-	-	3.64
		32.0	29.6	40.0	1.61076	
2	2098	0	0	-	-	3.80
		34.4	26.4	40.0	1.68235	
3	2098	0	53.6	62.8	0.85520	3.80
		21.6	16.8	28.8	2.75371	
4	2288	0	0	-	-	3.64
		40.8	40.8	49.6	1.16654	
5	2098	17.6	28.0	32.0	2.35116	3.80
		0	24.8	34.4	2.10945	

Table 4 — Results of measurements (Vickers hardness,L_1, L_2, L_3, L_4 - cracks' lengths, crack lengths from the center of the indentation to the end of the crack C, fracture toughness K_c and penetration depth h) for the indentations obtained with use of load of 4.905 N.

Indentation	HV	Cracks' lengths		C (μm)	K_c (MPa·m$^{1/2}$)	h (μm)
		L_1(μm)	L_2(μm)			
		L_3 (μm)	L_4 (μm)			
1	1968	11.2	78.4	55.2	1.33306	4.37
		13.6	20.0	28.0	3.68995	
2	1664	40.0	22.4	42.8	2.13329	4.77
		16.8	25.6	33.2	3.12254	
3	1915	36.0	40.0	49.2	1.61354	4.45
		0	0	-	-	
4	1722	28.8	42.4	47.2	1.81083	4.69
		52.0	25.6	50.4	1.64114	
5	2062	24.8	44.8	45.2	1.76576	4.29
		10.4	32.8	32.4	2.90952	

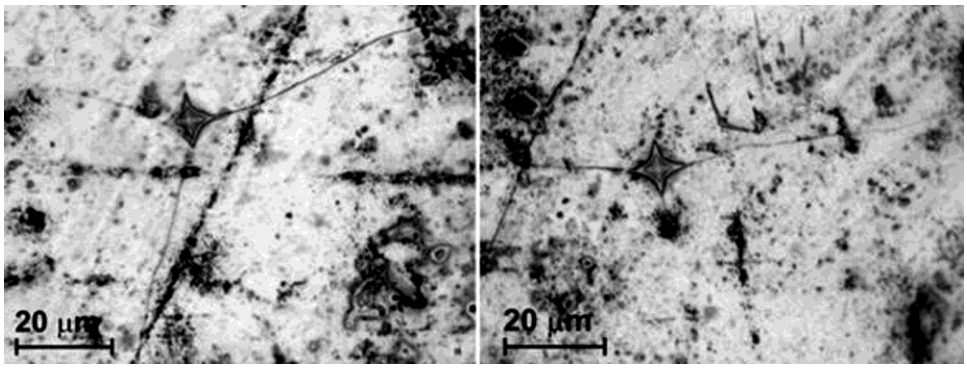

Fig. 7 — OM images of top-surface of plasma-paste borided layer formed on AISI D2 steel with visible indentation marks obtained with use of load of 1.962 N.

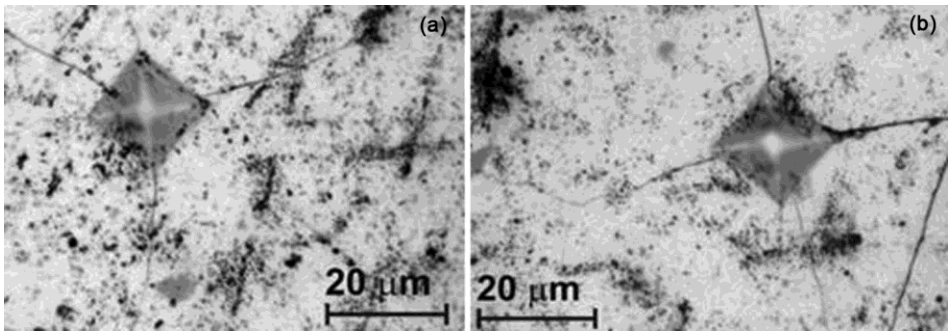

Fig. 8 — OM images of top-surface of plasma-paste borided layer formed on AISI D2 steel with visible indentation marks obtained with use of load of 3.924 N.

therefore very important was the calculation of penetration depth h of indenter during fracture toughness tests. The evaluated values of h were given also in Tables 2, 3, 4 and 5, for the corresponding values of indentation load: 1.962 N, 3.924 N, 4.905 N and 9.810 N. The following penetration depths were obtained: 2.58 μm, 3.74 μm, 4.51 μm and 8.55 μm for indentation loads of 1.962 N, 3.924 N, 4.905 N and 9.810 N, respectively. Of course, the penetration depth of indenter during fracture toughness measurements was calculated based on the diagonals of the indentation mark and angle of diamond pyramid α=136°. However, during hardness measurements, first, indenter penetrated to a highest depth – h_{max}, and then during unloading as a result of elastic recovery, the indentation depth could be reduced up to lower depth – h_p.

The schematic views of surface profiles under load and after load removal for indentation marks produced with different loads were presented in

Fig. 9. It was clearly visible that in case of low indentation loads both penetration depths (h_{max} and h_p) reached only FeB zone. Therefore, in case of low indentation loads (1.962 N and 3.924 N), the increase in load caused a decrease in fracture toughness. Other situation took place when higher loads (above 4.905 N) were applied during measurements. According to Fig. 9, during loading when indenter achieved maximal depth h_{max} the vertex of diamond pyramid penetrated the Fe_2B zone. After unloading, the elastic recovery caused change in the surface profile and penetration depth up to value h_p. Therefore, finally the whole cross-section of indentation mark was located only in FeB zone. However, the fact that during loading the indenter penetrated also the Fe_2B zone (in case of high indentation load also the transition zone) strongly influenced on obtained hardness and fracture toughness. It was easy observed that the cracks' lengths were lower for applied higher indentation loads (Tables 4 and 5). It was concluded that the values of K_C factor were depending on the applied indentation loads.

The determined fracture toughness was shown in Fig. 10 versus the indentation load. The two effects were clearly visible. First, the decrease in K_c values with increasing the indentation load up to 3.924 N, and second, the increase in fracture toughness with increasing the indentation load above 3.924 N. Similarly, in Fig. 11, the influence of indentation load on hardness was presented. In both cases, the critical value of load was 3.924 N. It could be concluded, that indentation load of 3.924 N was the value, above which the maximal depth h_{max} penetrated across Fe_2B zone/transition zone, according to Fig. 9. This situation was the reason for obtaining of diminished hardness (see Fig. 11) and increased

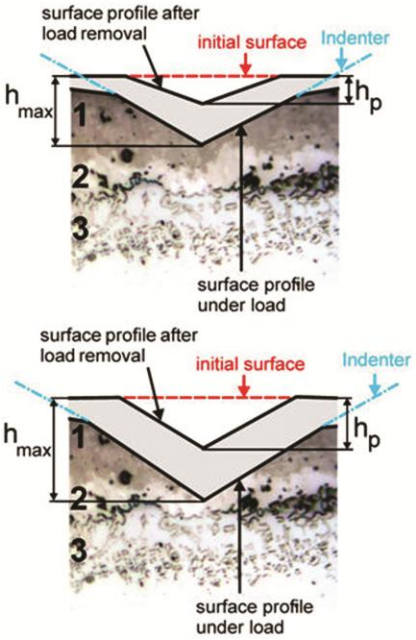

Fig. 9 — Schematic representation of the indenter-sample contact for low indentation loads (a) and high indentation loads (b); h_p - permanent indentation depth, h_{max} - maximum indentation depth, 1 – FeB zone, 2 – Fe_2B zone; 3 – transition zone.

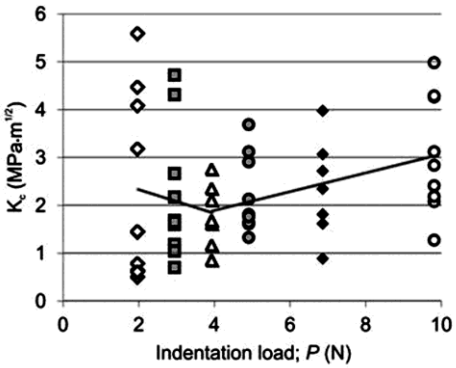

Fig. 10 — Fracture toughness of plasma-paste borided layer versus the applied indentation load.

Table 5 — Results of measurements (Vickers hardness,L_1, L_2, L_3, L_4 - cracks' lengths, crack lengths from the center of the indentation to the end of the crack C, fracture toughness K_c and penetration depth h) for the indentations obtained with use of load of 9.810 N.

Indentation	HV	Cracks' lengths		C (μm)	K_c (MPa·m$^{1/2}$)	h (μm)
		L_1(μm)	L_2(μm)			
		L_3 (μm)	L_4 (μm)			
1	1096	37.1	19.3	49.2	4.26682	8.32
		0	24.2	44.3	4.98374	
2	877	91.9	98.4	118.5	1.27476	9.30
		0	62.9	85.5	2.08183	
3	977	0	0	21.8	-	8.81
		19.3	62.9	62.9	3.12451	
4	1140	37.1	74.2	75.8	2.18679	8.16
		22.6	33.9	48.4	4.28817	
5	1140	29.0	72.6	70.9	2.41421	8.16
		0	43.5	63.7	2.83830	

fracture toughness. Probably, further increase in indentation load could still cause a higher decrease in hardness and simultaneously an increase in K_c value.

It was clearly visible in Fig. 11 that the differences between K_c values calculated for every indentation load were high. The reason for this situation could be the stress distribution in the borided layer. However, similarly effect was presented in paper[18]. In this work, the fracture toughness was measured by use of Berkovich indenter under a load ranged from 0.3 N to 0.5 N. The obtained results were summarized in Table 1. Depending on boriding process parameters, the calculated fracture toughness was ranged between 1.50 MPa·m$^{1/2}$ and 4.56 MPa·m$^{1/2}$ [18].

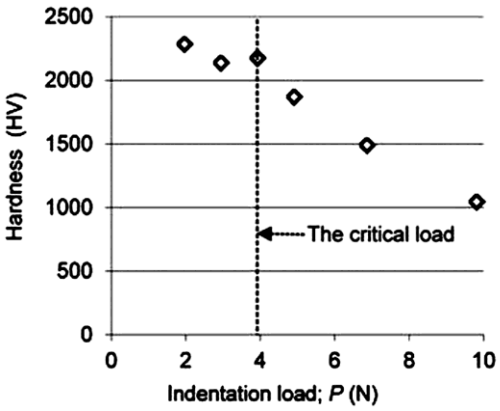

Fig. 11 — Hardness of plasma-paste borided layer versus the applied indentation load.

3.6 Cohesion test

The adhesion strength quality of the plasma-paste boride layers produced on AISI D2 steel was classified as HF3 standard (Fig. 12h), according to the VDI 3198 standard. The obtained indentation crater (Fig. 12a) with visible damages (Figs 12b and 12g) were analyzed. The radial cracks (Figs 12d and 12g) and little flaking areas at the perimeter of indentation craters were observed. This type and size of generated failures were characteristic of HF3 type of the adhesion strength quality. Therefore, the cohesion of plasma-paste borided layer was sufficient.

Several factors could influence on the cohesion strength of the boride layers. First, the high amount of FeB phase in the total boride layer since the FeB phase was known to be harder and more fragile than the Fe_2B phase. Moreover, the FeB phase was subjected to cracking and scaling under a mechanical strain because of the presence of tensile residual stresses[21]. Simultaneously, the formation of cracks is often occurred at the (FeB/Fe_2B) interface. The precipitation of chromium borides within the boronized layer could also increased the susceptibility to cracking. The last reason for diminished cohesion of plasma-paste borided layer was probably the high

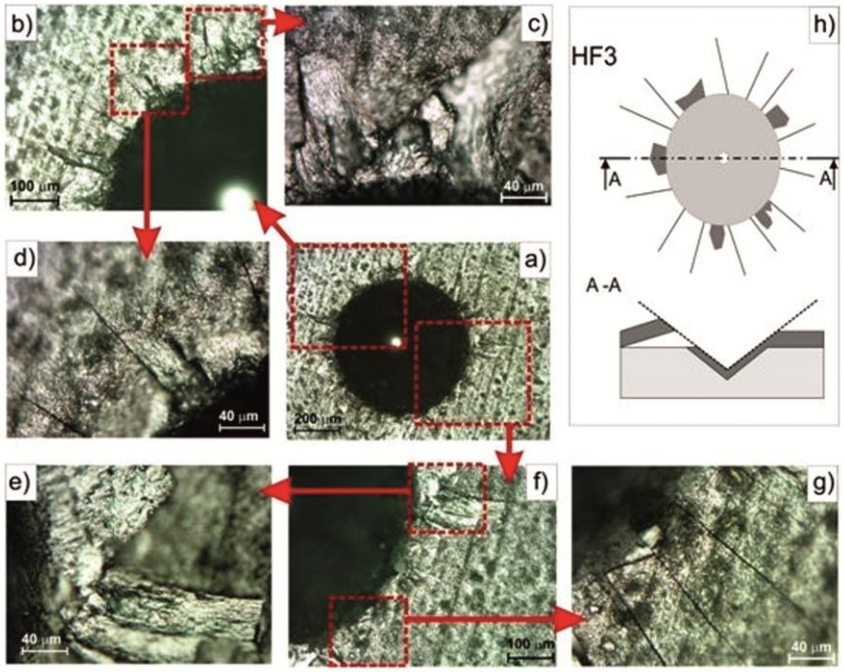

Fig. 12 — Rockwell-C indentations crater (a, b, f) with visible failures: (d, g) – radial microcracks, (c, e) – delamination, (h) the scheme of HF3 cohesion standard according with VDI 3198 norm.

hardness gradient between the produced layer and the material substrate. However, the obtained cohesion (HF3 standard) was an acceptable cohesion strength.

3.7 Kinetic studies

The kinetic data is needed for investigating the evolution of boronized layers on AISI D2 steel with the treatment time. It is known that the boriding kinetics is controlled by the diffusion of boron atoms at solid sate through the boride layer. Therefore, the thickness of boronized layer changes parabolically[24,25] with the treatment time expressed by Eq. (7):

$$u = \sqrt{Dt} \quad \ldots (7)$$

The variable u represents the thickness of boronized layer (in m), D the value of diffusion coefficient of boron at a given temperature (in $m^2\ s^{-1}$) and t the time duration (in s). The time dependence of total boride layer thickness for different boriding temperatures was shown in Fig. 13.

It is noticed that the thickness of total boride layer changes linearly with the square root of treatment time.

The evolution of the boron diffusion coefficient through the total boride layer in dependence of the boriding temperature is given by Equation (8) according to the Arrhenius relationship:

$$D = D_0 \exp(-\frac{Q}{RT}) \quad \ldots (8)$$

where , D_0 is a pre-exponential factor. The Q parameter represents the value of activation energy for boron diffusion in the AISI D2 steel.

This parameter is representative of the amount of energy (kJ mol^{-1}) necessary for the reaction to proceed, and R represents the ideal gas constant ($R=8.314\ Jmol^{-1}.K^{-1}$). The value of activation energy Q for boron diffusion can be easily obtained from the slope of the straight line giving $\ln(D)$ as a function of the reciprocal temperature.

The temperature dependence of boron diffusion coefficient through the total boride layer is depicted in Fig. 14.The obtained values of activation energies for boron diffusion in some borided steels[12,13,17,23,26-29] along with the value of activation energy found in this work (=130 kJ mol^{-1}) were gathered in Table 6. It was noticed that the collected values of boron activation energies from the literature are functions of the following various factors: (the boronizing method, the chemical composition of the substrate, the nature of boriding agent, chemical and electrochemical reactions involved during the boriding process). For

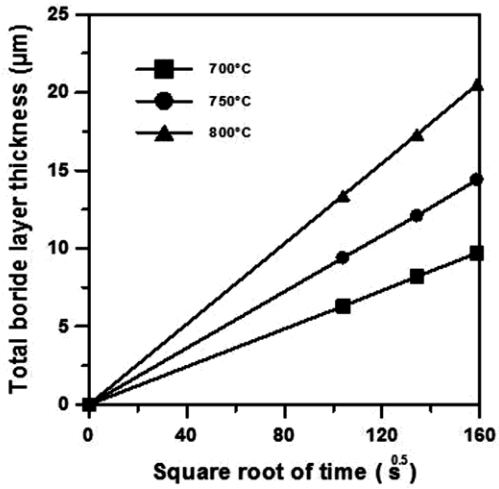

Fig. 13 — Variation of the boride layer thickness versus the square root of time for increasing temperatures.

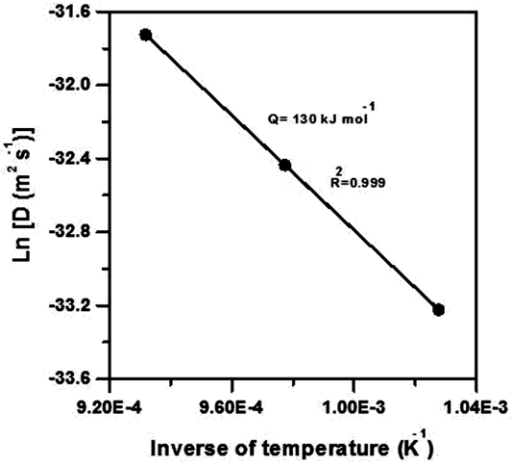

Fig. 14 — Temperature dependence of the boron diffusion coefficient through the total boride layer.

Table 6 — A comparison of values of activation energy for boron diffusion in AISI D2 steel with other steels using different boriding methods.

Material	Boriding method	Q (kJ mol^{-1})	References
AISI 304	Salt bath	253.35	26
AISI H13	Salt bath	244.37	26
AISI D2	Electrochemical boriding	137.86	17
AISI D2	Salt bath	170	23
AISI D2	Powder	201.5	27
AISI440C	Powder	340.42	28
AISI 51100	Plasma	106	29
AISI 8620	Plasma paste boriding	124.7-138.5	13
AISI 440 C	Plasma paste boriding	134.62	12
AISI D2	Plasma paste boriding	130.0	Present work

indication, the authors Sista *et al.* [17] have borided the AISI D2 steel using the electrochemical method in the range of 800-1000°C. They found a value of activation energy for boron diffusion equal to 137.86 kJ mol^{-1}. This value of energy was lower compared to the obtained value when pack-boriding the same steel[27]. In the case of boriding of the high-alloy steels[26-28], the thickness of boronized layer was reduced due to the effect of alloying elements. Therefore, the reported values of activation energy for boron diffusion were high in comparison with the values found for the plasma paste boriding. It was seen from Table 6 that plasma paste boriding[12,13] yielded a lower activation energy for boron diffusion in comparison with the conventional boriding methods[23,26,27,28].

In addition, Eq. (9) yielding the total boride layer thickness in dependence of the two parameters (the process temperature and the treatment time) can be used as an efficient tool to predict the optimized value of total boride layer thickness for practical utilization of boronized AISI D2 steel in the industry.

$$u = 188.86 \exp\left(-\frac{7820.3}{T}\right)\sqrt{t} \quad \ldots (9)$$

where u is expressed in (μm) , t represents the treatment time in (s) and T the absolute temperature in Kelvin.

4 Conclusions

In this study, the substrate made of AISI D2 steel was successfully plasma paste borided between 700 and 800 °C with exposure times of 3, 5 and 7 h using a mixture of (70% borax and 30% SiC) as a boron source. The main research results were given as follows:

(i) The interface between the boronized layer and transition zone was found to be flat. The boronized layer contained FeB and Fe_2B as well as CrB as precipitates, this result was based on XRD analysis. Moreover, the boronized layer was continuous and dense for all boriding conditions.

(ii) The boriding kinetics followed a parabolic regime and the thickness of boronized layer ranged from 6.3 μm to 20.5 μm.

(iii) The indentation test of Rockwell-C exhibited a cohesive quality of boronized layers on AISI D2 steel (obtained at 800°C for 7 h). The adhesion strength quality of the produced boride layers was classified according to HF3 category based on the 3198 VDI norm.

(iv) The values of fracture toughness measured on the plasma paste borided sample (at 800°C during 7 h) ranged from 0.504-5.706 MPa m$^{1/2}$ according to the chosen value of indentation load.

(v) The boron activation energy for AISI D2 steel was calculated as 130kJmol^{-1}. This value of energy was compared with the results reported in the literature data.

References

1 Sinha A K, *J Heat Treat*, 4 (1991) 437.
2 Keddam M, Kulka N, Makuch N, Pertek A & Małdziński L, *Appl Surf Sci*, 298 (2014) 115.
3 Mariani F E, Aureliano, R T Jr, Casteletti L C, Lombardi A N & Totten G E, *Mater Perform Charact*, 6 (2017) 523.
4 Zuno-Silva J, Ortiz-Domínguez M, Keddam M, Elias-Espinosa M, Damián-Mejía O, Cardoso-Legorreta E & Abreu-Quijano M, *J Min Metall Sect B-Metall*, 50 (2014) 101.
5 Nam K S, Lee K H, Lee S R & Kwon S C, *Surf Coat Technol*, 98 (1998) 886.
6 Gopalakrishnan P, Shankar P, Subba Rao R V, Sundar M & Ramakrishnan S S, *Scripta Mater*, 44 (5) (2001) 707.
7 Kulka M, Makuch N & Pertek A, *Optics Laser Technol*, 45 (2013) 308.
8 Kulka M, Mikolajczak D, Makuch N, Dziarski P & Miklaszewski A, *Surf Coat Technol*, 291 (2016) 292.
9 Yoon J H, Jee Y K & Lee S Y, *Surf Coat Technol*, 112 (1999) 71.
10 Ulker S, Gunes I & Taktak S, *Indian J Eng Mater Sci*, 18 (2011) 370.
11 Gunes I, Ulker S & Taktak S, *Mater Des*, 32 (2011) 2380.
12 Keddam M, Chegroune R, Kulka M, Panfil D, Ulker S & Taktak S, *Trans Indian Inst Met*, 70 (2017) 1377.
13 Gunes I, Taktak S, Bindal C, Yalcin Y, Ulker S & Kayali Y, Sadhana - Academy Proc Eng Sci, 38 (2013) 513.
14 Ucisik A H & Bindal C, *Surf Coat Technol*, 94-95 (1997) 561.
15 Kulka M, Makuch N & Piasecki A, *Surf Coat Technol*, 325 (2017) 515.
16 Verein Deutscher Ingenieure Normen, VDI 3198, VDI verlag (1991).
17 Sista V, Kahvecioglu O, Eryilmaz O L, Erdemir A & Timur S, *Thin Solid Films*, 520 (2011) 1582.
18 Rodriguez-Castro G, Campos-Silva I, Chavez-Gutierrez E, Martinez-Trinidad J, Hernandez-Sanchez E & Torres-Hernandez A, *Surf Coat Technol*, 215 (2013) 291.
19 Taktak S, *Mater Des*, 28 (2007) 1836.
20 Campos-Silva I, Ortiz-Domínguez M, Bravo-Bárcenas O, Doñu-Ruiz M A, Bravo-Bárcenas D, Tapia-Quintero C & Jiménez-Reyes M Y, *Surf Coat Technol*, 205 (2010) 403.
21 Kayali Y & Taktak S, *J Adh Sci Technol*, 29 (2015) 2065.
22 Kara R, Colak F & Kayali Y, *Trans Indian Inst Met*, 69 (2016) 1169.

23 Sen S, Sen U & Bindal C, *Surf Coat Technol*, 191 (2005) 274.
24 Tian X, Yang Y L, Sun S J, An J, Lu Y &Wang Z G, *J Mater Eng Perform*, 18 (2009) 162.
25 Ucar N, Aytar O B & Calik A, Mater Technol, 46 (2012) 621.
26 Taktak S, *J Mater Sci*, 41 (2006) 7590.
27 Ortiz-Domínguez M, Keddam M, Elias-Espinosa M, Damián-Mejía O, Flores-Rentería M A, Arenas-Flores A & Hernández-Ávila J, *Surf Eng*, 30 (2014) 490.
28 Kayali Y, Günes I & Ulu S, *Vacuum*, 86 (2012) 1428.
29 Ipek M, Celebi Efe G, Ozbek I, Zeytin S & Bindal C, *J Mater Eng Perform*, 21 (2012) 733.